ISSN 0915-633X

NATIONAL INSTITUTE FOR FUSION SCIENCE

Second Order Focusing Property of 210° Cylindrical Energy Analyzer

A. Fujisawa, H. Iguchi, M. Sasao and Y. Hamada

(Received - Oct. 7, 1994)

NIFS-317 Nov. 1994

RESEARCH REPORT
NIFS Series

NAGOYA, JAPAN

Second Order Focusing Property of 210° Cylindrical Energy Analyzer

A. Fujisawa, H. Iguchi, M. Sasao, Y. Hamada

National Institute for Fusion Science
Furo-cho, Chikusa-ku, Nagoya, Japan

Abstract

It was confirmed experimentally that a 210° cylindrical energy analyzer with drift spaces has second order focusing. The properties of the analyzer is deeply dependent on the fringing field around the entrance and exit of the cylinders.

Keywords: 210° cylindrical energy analyzer, second order focusing, fringing field

I. Introduction

Electrostatic energy analyzers, such as 127.3° cylindrical energy analyzer[1,2], 30° parallel plate energy analyzer[3,4] , are widely used in many scientific fields owing to its simple and economical structure. Particularly, 30° parallel plate analyzer has excellent properties in terms of both energy resolution and the focusing property of the beam incident angle. These properties have made the 30° parallel plate energy analyzer utilized for the heavy ion beam probe which provides a unique method of diagnosing the electrostatic potential of the magnetically confined plasma with high electron temperature. However, the operational voltage of the parallel plate analyzer becomes closer to the practical limit as the necessary beam energy approaches to more than several MeV region[5,6].

On the other hand, the cylindrical analyzer has a potential to be the analyzer for the MeV range heavy ion beam probe since the operation voltage can be smaller due to the efficient use of the electric field. However, the acceptance angle width of the cylindrical energy analyzer is insufficient for this use; this analyzer has an only first order focusing, while the 30° parallel plate does second order focusing. The theoretical analysis[7] was executed to examine the possibility that the cylindrical analyzer should have second order focusing by adding drift spaces at both ends of the cylinders, similarly to the parallel plate analyzer. The result showed that cylindrical energy analyzers whose angle length are more than 127.3° should have second order focusing, although the energy resolution should be deteriorated. A cylindrical analyzer with angle length of 210° was constructed in order to verify the proposition. This article will report the preliminary results of the second

order focusing property and the energy resolution obtained in the cylindrical energy analyzer.

II. 210° Cylindrical Energy Analyzer

The schematic view of the 210° cylindrical energy analyzer is illustrated in Fig. 1. The geometrical parameters in Fig. 1a are R_0=150mm, R_p=168mm, R_n=132mm. The thickness and height of the cylindrical electrodes, which are made of aluminum, are 12mm, 120mm, respectively. The positions of the entrance slit and detector are movable to search better analyzer properties; $H = 0 \sim 90$mm, $L = 30 \sim 120$mm. The height and width of the entrance slit are chosen to be 10.0mm, 0.5mm, respectively. In order to change the beam entrance angle, the energy analyzer is set on the table which is rotated around the entrance slit position. The system permits us to investigate the dependence of the beam displacement on the beam incident angle $\Delta R(\Delta\theta)$.

The theoretical analysis assumes that the fringing fields around the ends of the cylinder are completely confined within finite region represented by Δ_f in Fig. 1; here it is chosen to be $\Delta_f = 15$mm. In order to satisfy this requirement, wires of 0.1mm diameter are spaced every 1mm on two rectangular holes in the entrance and the exit (see Fig. 1c). The penetration of the fringing field to the outside should be minimized. Moreover, boundary conditions are important to determine the fringing field structure. Two cylindrical boards grounded to the vacuum chamber are placed to determine the inner electrical boundary. They are located at the exact opposite position of the the vacuum chamber outer wall around the center of the cylinder; both are 75mm far from the center radius.

The split plates detector is used since it has sufficient sensitivity to small beam displacement. With the assumption of the uniform beam current profile, the displacement ΔR of the beam on the split plates is associated with the detected current difference as follows,

$$\Delta R = \frac{w}{2}\left(\frac{i_{\rm out} - i_{\rm in}}{i_{\rm out} + i_{\rm in}}\right) , \tag{1}$$

where $i_{\rm out}$, $i_{\rm in}$ and w are the currents on the outside, the inside plates and the entrance slit width, respectively. The position of the center cut of the split plates is supposed to affect the analyzer property. We prepared, as a result, several split plates which have the center cuts at the different position $R_{\rm s}$; $\Delta R_{\rm s}(= R_{\rm s} - R_0) = 0.0, \pm 0.5, \pm 1.0, \pm 1.5$mm.

III. Experimental Results

This energy analyzer is divided into three characteristic regions; (1) centrifugal electric field (2) fringing field (3) field free regions. The electric field strength and potential in the centrifugal region are described as

$$E_r(R) = \frac{E_{r0}R_0}{R} , \tag{2}$$

$$\psi(R) = E_{\rm r0}R_0 \log(R/R_0) + \psi_0 , \tag{3}$$

respectively, and

$$E_{\rm r0} = \frac{V_{\rm p} - V_{\rm n}}{R_0 \log\left(R_{\rm p}/R_{\rm n}\right)} \tag{4}$$

$$\psi_0 = \frac{V_{\rm n}\log(R_{\rm p}/R_0) - V_{\rm p}\log(R_{\rm n}/R_0)}{\log(R_{\rm p}/R_{\rm n})} . \tag{5}$$

where $V_{\rm p}$, $V_{\rm n}$ represent the voltages on the outside and inside electrodes, respectively. The charged particle motion in the centrifugal field region depends on only the electric field $E_r(R)$. However, the initial condition of the

particle motion is affected seriously by $\psi(R)$ since the particle will obtain the potential energy and change its velocity before entering the centrifugal electric field region. Consequently, the analyzer properties are determined by four parameter sets; $V_{\rm p}$, $V_{\rm n}$, H, L. Thus, the displacement of the beam on the split plate detector is generally expressed in the Taylor expansion form as

$$\Delta r = \frac{\Delta R}{R_0} = C_0(H,\ L,\ V_{\rm p},\ V_{\rm n}) + C_1(H,\ L, V_{\rm p},\ V_{\rm n})\delta\theta + C_2(H,\ L,\ V_{\rm p},\ V_{\rm n})\delta\theta^2 + \cdots + \frac{\partial R}{\partial E}\delta E + \cdots\ , \tag{6}$$

where $\partial R/\partial E$ means the energy resolution, and the first through the third terms dependent on the incident angle $\delta\theta$ represent the focus property. The condition of the second order focusing is defined by

$$C_1 = C_2 = 0\ . \tag{7}$$

The characteristics of the ideal 127.3° energy analyzer in the Taylor expansion form is described as

$$\Delta r = -\frac{4}{3}\delta\theta^2 + \cdots + \delta E + \cdots, \tag{8}$$

where the first order focusing condition is satisfied; $C_1 = 0$, $C_2 \neq 0$.

The procedure to find the second order focusing with different entrance distances H and different slit plate positions $R_{\rm s}$ was executed using a 10keV Cs^+ ion beam source located about 5m away from the analyzer. The second order focusing could be realized only when the center position of the split plate was located at 0.5mm outside from the center ($R_{\rm s}$ = 150.5mm). When the center of the split plate detector was located at 0.0mm, -0.5mm, ±1.0mm

or ± 1.5mm from the center line, the second order focusing could never be found so far.

Figure 2 shows the dependence of normalized beam displacement $\Delta r = \Delta R/R_0$ on the beam entrance angle for two cases of $H = 45.0$mm, 50.0mm. The close circles show the case of $H = 45.0$mm, $L = 55.0$mm, $V_{\rm p} = 2.636$kV, $V_{\rm n} = -2.414$kV. Then Eqs. (4, 5) yield $E_{\rm r0} = 139.6$kV/m, $\psi_0 = 0.263$kV. The least square method gives the fitting polynomial functions to this case as

$$\Delta r = -0.029\delta\theta^2 + 1.644\delta\theta^3 - 1.861\delta\theta^4 + \cdots . \tag{9}$$

The open circles show the case of $H = 50$mm, $L = 60.0$mm with $V_{\rm p}$=2.273kV, $V_{\rm n} = -3.055$kV, or $E_{\rm r0} = 147.3$kV/m, $\psi_0 = -0.231$kV. The fitting function of this case is then

$$\Delta r = -0.022\delta\theta^2 + 1.927\delta\theta^3 - 1.363\delta\theta^4 + \cdots . \tag{10}$$

For these two cases, the dependence of the displacement on the beam energy is indicated in Fig. 3. The fitting functions of $H = 45.0$mm, 50.0mm are

$$\Delta r = -0.017\delta\epsilon - 0.33\delta\epsilon^2 + \cdots , \tag{11}$$

$$\Delta r = -0.020\delta\varepsilon - 0.252\delta\varepsilon^2 + \cdots , \tag{12}$$

respectively. Thus, the energy resolution is about -0.02. The value is much smaller than that of the 127.3° cylindrical analyzer; theoretically 1.

Figure 4 shows the dependence of the focusing property on the voltages for the case of $H = 45.0$mm, $L = 55$mm. The reference curve, which has been already shown in Fig. 2, is represented by the close circles. The open circles show the case of $V_{\rm p} = 2.641$kV, $V_{\rm n} = -2.404$kV ($E_{\rm r0} = 139.5$kV/m,

ψ_0=0.270kV). Then the dependence of the displacement on the beam incident angle is expressed as

$$\Delta r = 0.003\delta\theta - 0.034\delta\theta^2 + 1.710\delta\theta^3 - 1.667\delta\theta^4 + \cdots. \tag{13}$$

The squares indicate the case with $V_{\rm p} = 2.631$kV, $V_{\rm n} = -2.434$kV ($E_{\rm r0} = 140.0$kV/m, $\psi_0 = 0.251$kV), and the characteristic curve is

$$\Delta r = -0.002\delta\theta - 0.033\delta\theta^2 + 1.617\delta\theta^3 - 1.380\delta\theta^4 + \cdots \tag{14}$$

These two cases indicate that very small change of the voltages ($\Delta V_{\rm p} \simeq 5$V, $V_{\rm n} \simeq 10 \sim 20$V) gives a finite first order coefficient.

Here, we demonstrated two cases where the second order focusing was found. The following consideration proves that in vicinity of these cases there should be other parameters to be consistent with the second order focusing. By differentiating the Eq. (6) around the parameter giving second order focusing, we obtain

$$\frac{\partial C_0}{\partial H}\Delta H + \frac{\partial C_0}{\partial L}\Delta L + \frac{\partial C_0}{\partial V_{\rm p}}\Delta V_{\rm p} + \frac{\partial C_0}{\partial V_{\rm n}}\Delta V_{\rm n} = 0 \tag{15}$$

$$\frac{\partial C_1}{\partial H}\Delta H + \frac{\partial C_1}{\partial L}\Delta L + \frac{\partial C_1}{\partial V_{\rm p}}\Delta V_{\rm p} + \frac{\partial C_1}{\partial V_{\rm n}}\Delta V_{\rm n} = 0 \tag{16}$$

$$\frac{\partial C_2}{\partial H}\Delta H + \frac{\partial C_2}{\partial L}\Delta L + \frac{\partial C_2}{\partial V_{\rm p}}\Delta V_{\rm p} + \frac{\partial C_2}{\partial V_{\rm n}}\Delta V_{\rm n} = 0 \tag{17}$$

Corresponding to a finite change of ΔH, it is possible to find the other parameters ΔL, $\Delta V_{\rm p}$, $\Delta V_{\rm n}$ to satisfy the above relations. Therefore, it is expected that we should find the other parameters to realize the second order focusing around the region from $H = 45$mm to $H = 50$mm.

IV. Comparison with Theoretical Expectation

The theoretical analysis[7] assumed the electric field parameters defined in Eqs. (2-5)

$$E_{r0} = \frac{2K_0}{R_0 q}, \quad \psi_0 = 0 \tag{18}$$

where K_0, q represent the beam energy, the charge, respectively. A rather simple fringing field was adopted to give an explicit analytic solution to the beam trajectory in the region Δ_f. Under the conditions of $\Delta_f = 0.1R_0 =$ 15mm, the theory predicted that the second order focusing should be achieved when $H = 0.160R_0 = 24$mm, $L = 0.552R_0 = 82.8$mm, $\Delta R_s = -0.0113R_0 =$ -1.6mm. Then, the focusing characteristics and the energy resolution are given as

$$\Delta r = 0.15\delta\theta^3 - 0.36\delta\theta^4 + \cdots , \tag{19}$$

$$\Delta r = -0.16\delta\varepsilon - 0.14\delta\varepsilon^2 + \cdots , \tag{20}$$

respectively.

In our experiments the second order focus was realized, however, it was not when these predicted parameters. The actual analyzer allows more variety in the combination of the voltages and the location of the split plates. If compare Eqs. (9-14) with Eqs. (19, 20), the obtained properties are worse than the theoretical ones in terms of both energy resolution and the beam acceptance angle (indicated by third order coefficient C_3). Thus, the experiment results are consistent with the theory qualitatively but not quantitatively.

This discrepancy should be ascribed to the difference between the actual and the theoretically assumed fringing fields. We searched the second order focusing with no inner boundary board for all split plate locations. In this case, we could never find any parameters to satisfy the second order focusing,

although the first order focusing could be easily obtained for wide ranges of H and L by adjusting the voltages $V_{\rm p}$, $V_{\rm n}$. The second order coefficient always had a negative value $C_2 < 0$; the characteristic curve was always parabolic. In the case with the boundary board, the second order could be realized only for the special split plate location $R_{\rm s} = 150.5$mm. These results indicate that the fringing field plays a very essential role on the analyzer properties. Therefore, we consider that these properties obtained here should not be final and can be improved. More appropriate fringing field will be arranged by changing the location of the boundary boards and the structure of the cylindrical electrodes around the edges.

References

[1] A. L. Hughes, V. Rojanski, Phys. Rev. **34**, 284(1929).

[2] A. L. Hughes, J. H. McMillen, Phys. Rev. **34**, 291(1929).

[3] T. S. Green and G. A. Proca, Rev. Sci. Instrum. **41**, 1409(1970).

[4] G. A. Proca and T. S. Green, Rev. Sci. Instrum. **41**, 1778(1970).

[5] R. L. Hickok, W. C. Jennings, K. A. Connor, P. M. Schock, Rev. Sci. Instrum. **56**, 1047(1985).

[6] A. Fujisawa, H. Iguchi, A. Taniike, M. Sasao, Y. Hamada, IEEE, Trans. of Plasma Sci. **22**, 395(1994).

[7] A. Fujisawa, Y. Hamada, Rev. Sci. Instrum. **64**, 3503(1993).

Figure Captions

Fig. 1: (a) Schematic view of 210° cylindrical energy analyzer (b) split plate detector (c) rectangular holes with wires spaced on.

Fig. 2: Two cases with second order focusing properties. The closed circles show the characteristic curve $H = 45.0$mm, $L = 55.0$mm, and the open circles do that of $H = 50.0$mm,$L = 60.0$mm.

Fig. 3: Energy resolutions of the cases shown in Fig. 2. The closed and open circles shows those of $H = 45.0$mm $L = 55.0$mm, $H = 50.0$mm $L = 60.0$mm, respectively.

Fig. 4: Dependence of focusing property on the voltages for the case of $H = 45.0$mm, $L = 55.0$mm. The closed circles represent the same curve as that shown in Fig. 2.

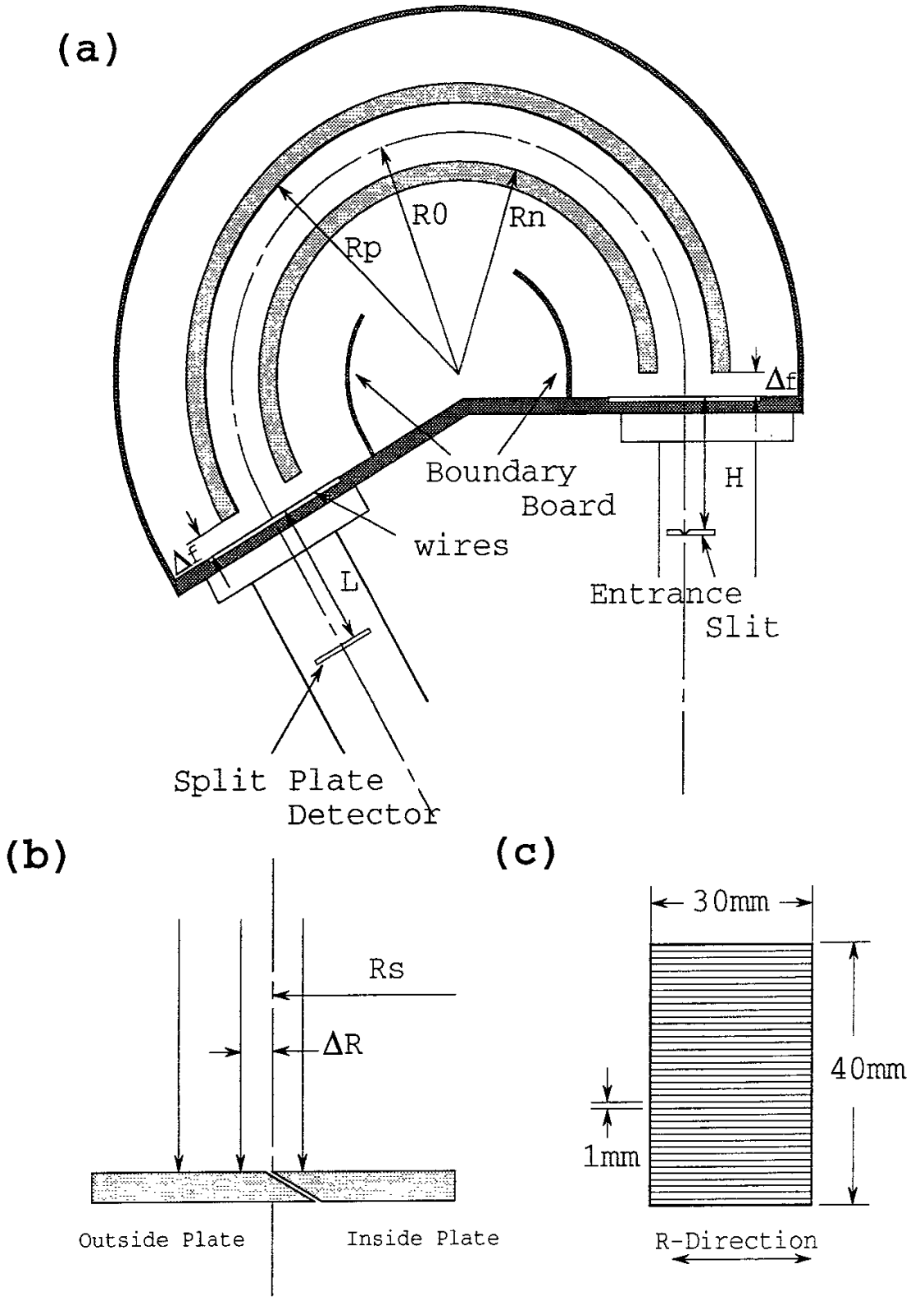

Fig. 1 A. Fujisawa, H. Iguchi, M. Sasao, Y. Hamada

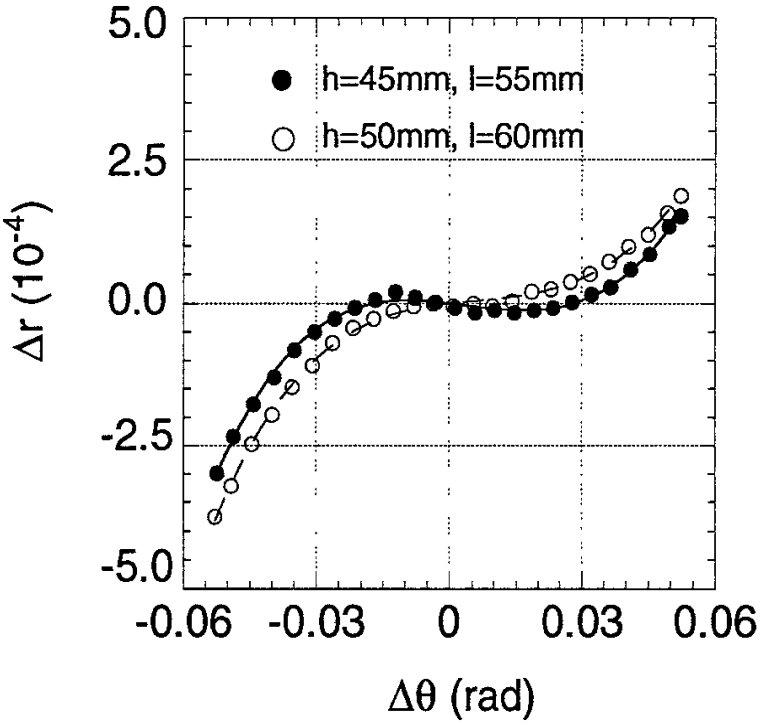

Fig. 2 A. Fujisawa, H. Iguchi, M. Sasao, Y. Hamada

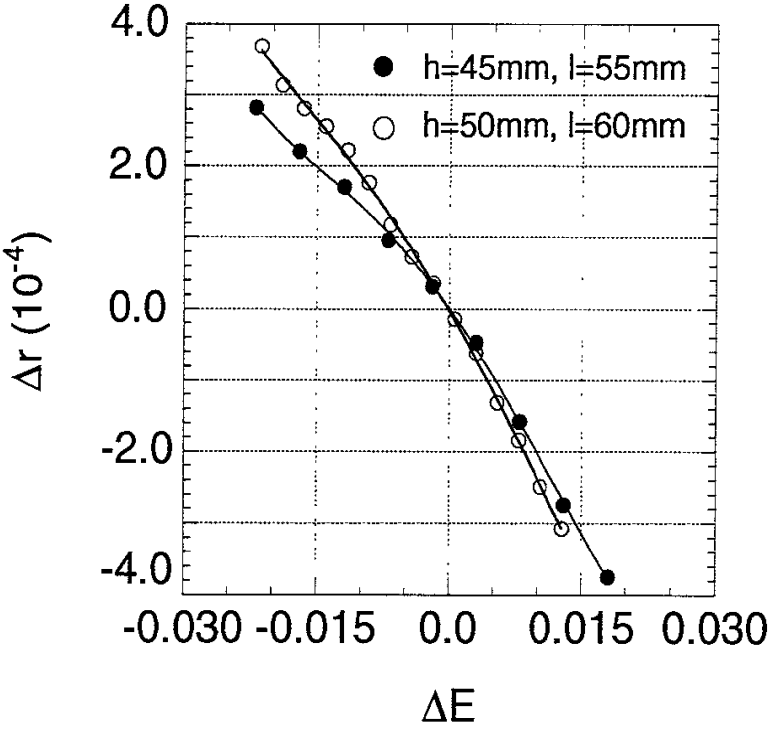

Fig. 3 A. Fujisawa, H. Iguchi, M. Sasao, Y. Hamada

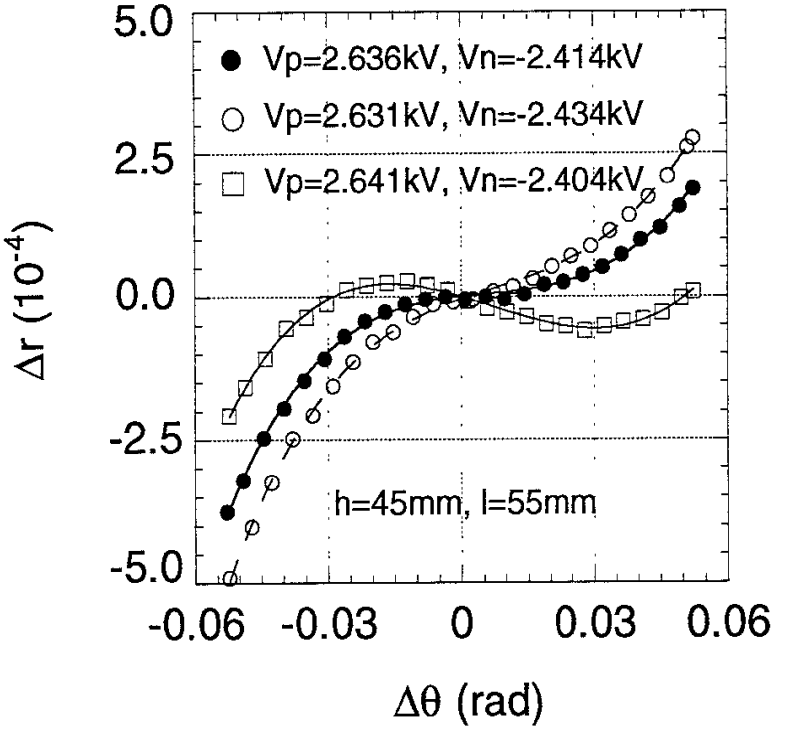

Fig. 4 A. Fujisawa, H. Iguchi, M. Sasao, Y. Hamada

Recent Issues of NIFS Series

NIFS-279 K. Yamazaki and K.Y.Watanabe,
New Modular Heliotron System Compatible with Closed Helical Divertor and Good Plasma Confinement; Apr. 1994

NIFS-280 S. Okamura, K. Matsuoka, K. Nishimura, K. Tsumori, R. Akiyama, S. Sakakibara, H. Yamada, S. Morita, T. Morisaki,. N. Nakajima, K. Tanaka, J. Xu, K. Ida, H. Iguchi, A. Lazaros, T. Ozaki, H. Arimoto, A. Ejiri, M. Fujiwara, H. Idei. O. Kaneko, K. Kawahata, T. Kawamoto, A. Komori, S. Kubo, O. Motojima, V.D. Pustovitov, C. Takahashi, K. Toi and I. Yamada,
High-Beta Discharges with Neutral Beam Injection in CHS; Apr. 1994

NIFS-281 K. Kamada, H. Kinoshita and H. Takahashi,
Anomalous Heat Evolution of Deuteron Implanted Al on Electron Bombardment ; May 1994

NIFS-282 H. Takamaru, T. Sato, K. Watanabe and R. Horiuchi,
Super Ion Acoustic Double Layer; May 1994

NIFS-283 O.Mitarai and S. Sudo
Ignition Characteristics in D-T Helical Reactors; June 1994

NIFS-284 R. Horiuchi and T. Sato,
Particle Simulation Study of Driven Magnetic Reconnection in a Collisionless Plasma; June 1994

NIFS-285 K.Y. Watanabe, N. Nakajima, M. Okamoto, K. Yamazaki, Y. Nakamura, M. Wakatani,
Effect of Collisionality and Radial Electric Field on Bootstrap Current in LHD (Large Helical Device); June 1994

NIFS-286 H. Sanuki, K. Itoh, J. Todoroki, K. Ida, H. Idei, H. Iguchi and H. Yamada,
Theoretical and Experimental Studies on Electric Field and Confinement in Helical Systems; June 1994

NIFS-287 K. Itoh and S-I. Itoh,
Influence of the Wall Material on the H-mode Performance; June 1994

NIFS-288 K. Itoh, A. Fukuyama, S.-I. Itoh, M. Yagi and M. Azumi
Self-Sustained Magnetic Braiding in Toroidal Plasmas: July 1994

NIFS-289 Y. Nejoh,
Relativistic Effects on Large Amplitude Nonlinear Langmuir Waves in a Two-Fluid Plasma; July 1994

NIFS-290 N. Ohyabu, A. Komori, K. Akaishi, N. Inoue, Y. Kubota, A.I. Livshit,

N. Noda, A. Sagara, H. Suzuki, T. Watanabe, O. Motojima, M. Fujiwara, A. Iiyoshi,
Innovative Divertor Concepts for LHD; July 1994

NIFS-291 H. Idei, K. Ida, H. Sanuki, S. Kubo, H. Yamada, H. Iguchi, S. Morita, S. Okamura, R. Akiyama, H. Arimoto, K. Matsuoka, K. Nishimura, K. Ohkubo, C. Takahashi, Y. Takita, K. Toi, K. Tsumori and I. Yamada,
Formation of Positive Radial Electric Field by Electron Cyclotron Heating in Compact Helical System; July 1994

NIFS-292 N. Noda, A. Sagara, H. Yamada, Y. Kubota, N. Inoue, K. Akaishi, O. Motojima, K. Iwamoto, M. Hashiba, I. Fujita, T. Hino, T. Yamashina, K. Okazaki, J. Rice, M. Yamage, H. Toyoda and H. Sugai,
Boronization Study for Application to Large Helical Device; July 1994

NIFS-293 Y. Ueda, T. Tanabe, V. Philipps, L. Könen, A. Pospieszczyk, U. Samm, B. Schweer, B. Unterberg, M. Wada, N. Hawkes and N. Noda,
Effects of Impurities Released from High Z Test Limiter on Plasma Performance in TEXTOR; July. 1994

NIFS-294 K. Akaishi, Y. Kubota, K. Ezaki and O. Motojima,
Experimental Study on Scaling Law of Outgassing Rate with A Pumping Parameter, Aug. 1994

NIFS-295 S. Bazdenkov, T. Sato, R. Horiuchi, K. Watanabe
Magnetic Mirror Effect as a Trigger of Collisionless Magnetic Reconnection, Aug. 1994

NIFS-296 K. Itoh, M. Yagi, S.-I. Itoh, A. Fukuyama, H. Sanuki, M. Azumi
Anomalous Transport Theory for Toroidal Helical Plasmas,
Aug. 1994 (IAEA-CN-60/D-III-3)

NIFS-297 J. Yamamoto, O. Motojima, T. Mito, K. Takahata, N. Yanagi, S. Yamada, H. Chikaraishi, S. Imagawa, A. Iwamoto, H. Kaneko, A. Nishimura, S. Satoh, T. Satow, H. Tamura, S. Yamaguchi, K. Yamazaki, M. Fujiwara, A. Iiyoshi and LHD group,
New Evaluation Method of Superconductor Characteristics for Realizing the Large Helical Device; Aug. 1994 (IAEA-CN-60/F-P-3)

NIFS-298 A. Komori, N. Ohyabu, T. Watanabe, H. Suzuki, A. Sagara, N. Noda, K. Akaishi, N. Inoue, Y. Kubota, O Motojima, M. Fujiwara and A. Iiyoshi,
Local Island Divertor Concept for LHD; Aug. 1994 (IAEA-CN-60/F-P-4)

NIFS-299 K. Toi, T. Morisaki, S. Sakakibara, A. Ejiri, H. Yamada, S. Morita, K. Tanaka, N. Nakajima, S. Okamura, H. Iguchi, K. Ida, K. Tsumori, S. Ohdachi, K. Nishimura, K. Matsuoka, J. Xu, I. Yamada, T. Minami, K. Narihara, R. Akiyama, A. Ando, H. Arimoto, A. Fujisawa, M. Fujiwara, H. Idei, O. Kaneko, K. Kawahata, A. Komori, S. Kubo, R. Kumazawa, T. Ozaki, A. Sagara, C. Takahashi, Y. Takita and T. Watari

Impact of Rotational-Transform Profile Control on Plasma Confinement and Stability in CHS; Aug. 1994 (IAEA-CN-60/A6/C-P-3)

NIFS-300 H. Sugama and W. Horton,
Dynamical Model of Pressure-Gradient-Driven Turbulence and Shear Flow Generation in L-H Transition; Aug. 1994 (IAEA/CN-60/D-P-I-11)

NIFS-301 Y. Hamada, A. Nishizawa, Y. Kawasumi, K.N. Sato, H. Sakakita, R. Liang, K. Kawahata, A. Ejiri, K. Narihara, K. Sato, T. Seki, K. Toi, K. Itoh, H. Iguchi, A. Fujisawa, K. Adachi, S. Hidekuma, S. Hirokura, K. Ida, M. Kojima, J. Koog, R. Kumazawa, H. Kuramoto, T. Minami, I. Negi, S. Ohdachi, M. Sasao, T. Tsuzuki, J. Xu, I. Yamada, T. Watari,
Study of Turbulence and Plasma Potential in JIPP T-IIU Tokamak; Aug. 1994 (IAEA/CN-60/A-2-III-5)

NIFS-302 K. Nishimura, R. Kumazawa, T. Mutoh, T. Watari, T. Seki, A. Ando, S. Masuda, F. Shinpo, S. Murakami, S. Okamura, H. Yamada, K. Matsuoka, S. Morita, T. Ozaki, K. Ida, H. Iguchi, I. Yamada, A. Ejiri, H. Idei, S. Muto, K. Tanaka, J. Xu, R. Akiyama, H. Arimoto, M. Isobe, M. Iwase, O. Kaneko, S. Kubo, T. Kawamoto, A. Lazaros, T. Morisaki, S. Sakakibara, Y. Takita, C. Takahashi and K. Tsumori,
ICRF Heating in CHS; Sep. 1994 (IAEA-CN-60/A-6-I-4)

NIFS-303 S. Okamura, K. Matsuoka, K. Nishimura, K. Tsumori, R. Akiyama, S. Sakakibara, H. Yamada, S. Morita, T. Morisaki, N. Nakajima, K. Tanaka, J. Xu, K. Ida, H. Iguchi, A. Lazaros, T. Ozaki, H. Arimoto, A. Ejiri, M. Fujiwara, H. Idei, A. Iiyoshi, O, Kaneko, K. Kawahata, T. Kawamoto, S. Kubo, T. Kuroda, O. Motojima, V.D. Pustovitov, A. Sagara, C. Takahashi, K. Toi and I. Yamada,
High Beta Experiments in CHS; Sep. 1994 (IAEA-CN-60/A-2-IV-3)

NIFS-304 K. Ida, H. Idei, H. Sanuki, K. Itoh, J. Xu, S. Hidekuma, K. Kondo, A. Sahara, H. Zushi, S.-I. Itoh, A. Fukuyama, K. Adati, R. Akiyama, S. Bessho, A. Ejiri, A. Fujisawa, M. Fujiwara, Y. Hamada, S. Hirokura, H. Iguchi, O. Kaneko, K. Kawahata, Y. Kawasumi, M. Kojima, S. Kubo, H. Kuramoto, A. Lazaros, R. Liang, K. Matsuoka, T. Minami, T. Mizuuchi, T. Morisaki, S. Morita, K. Nagasaki, K. Narihara, K. Nishimura, A. Nishizawa, T. Obiki, H. Okada, S. Okamura, T. Ozaki, S. Sakakibara, H. Sakakita, A. Sagara, F. Sano, M. Sasao, K. Sato, K.N. Sato, T. Saeki, S. Sudo, C. Takahashi, K. Tanaka, K. Tsumori, H.Yamada, I. Yamada, Y. Takita, T. Tuzuki, K. Toi and T. Watari,
Control of Radial Electric Field in Torus Plasma; Sep. 1994 (IAEA-CN-60/A-2-IV-2)

NIFS-305 T. Hayashi, T. Sato, N. Nakajima, K. Ichiguchi, P. Merkel, J. Nührenberg, U. Schwenn, H. Gardner, A. Bhattacharjee and C.C.Hegna,
Behavior of Magnetic Islands in 3D MHD Equilibria of Helical Devices; Sep. 1994 (IAEA-CN-60/D-2-II-4)

NIFS-306 S. Murakami, M. Okamoto, N. Nakajima, K.Y. Watanabe, T. Watari, T. Mutoh, R. Kumazawa and T. Seki,
Monte Carlo Simulation for ICRF Heating in Heliotron/Torsatrons;
Sep. 1994 (IAEA-CN-60/D-P-I-14)

NIFS-307 Y. Takeiri, A. Ando, O. Kaneko, Y. Oka, K. Tsumori, R. Akiyama, E. Asano, T. Kawamoto, T. Kuroda, M. Tanaka and H. Kawakami
Development of an Intense Negative Hydrogen Ion Source with a Wide-Range of External Magnetic Filter Field; Sep. 1994

NIFS-308 T. Hayashi, T. Sato, H.J. Gardner and J.D. Meiss,
Evolution of Magnetic Islands in a Heliac; Sep. 1994

NIFS-309 H. Amo, T. Sato and A. Kageyama,
Intermittent Energy Bursts and Recurrent Topological Change of a Twisting Magnetic Flux Tube; Sep.1994

NIFS-310 T. Yamagishi and H. Sanuki,
Effect of Anomalous Plasma Transport on Radial Electric Field in Torsatron/Heliotron; Sep. 1994

NIFS-311 K. Watanabe, T. Sato and Y. Nakayama,
Current-profile Flattening and Hot Core Shift due to the Nonlinear Development of Resistive Kink Mode; Oct. 1994

NIFS-312 M. Salimullah, B. Dasgupta, K. Watanabe and T. Sato,
Modification and Damping of Alfvén Waves in a Magnetized Dusty Plasma; Oct. 1994

NIFS-313 K. Ida, Y. Miura, S -I. Itoh, J.V. Hofmann, A. Fukuyama, S. Hidekuma, H. Sanuki, H. Idei, H. Yamada, H. Iguchi, K. Itoh,
Physical Mechanism Determining the Radial Electric Field and its Radial Structure in a Toroidal Plasma; Oct. 1994

NIFS-314 Shao-ping Zhu, R. Horiuchi, T. Sato and The Complexity Simulation Group,
Non-Taylor Magnetohydrodynamic Self-Organization; Oct. 1994

NIFS-315 M. Tanaka,
Collisionless Magnetic Reconnection Associated with Coalescence of Flux Bundles; Nov. 1994

NIFS-316 M. Tanaka,
Macro-EM Particle Simulation Method and A Study of Collisionless Magnetic Reconnection; Nov. 1994